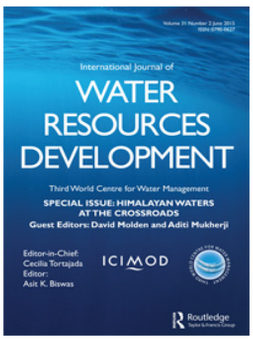

International Journal of Water Resources Development

ISSN: 0790-0627 (Print) 1360-0648 (Online) Journal homepage: https://www.tandfonline.com/loi/cijw20

A comparative high-altitude meteorological analysis from three catchments in the Nepalese Himalaya

J.M. Shea, P. Wagnon, W.W. Immerzeel, R. Biron, F. Brun & F. Pellicciotti

To cite this article: J.M. Shea, P. Wagnon, W.W. Immerzeel, R. Biron, F. Brun & F. Pellicciotti (2015) A comparative high-altitude meteorological analysis from three catchments in the Nepalese Himalaya, International Journal of Water Resources Development, 31:2, 174-200, DOI: 10.1080/07900627.2015.1020417

To link to this article: https://doi.org/10.1080/07900627.2015.1020417

Published online: 18 Apr 2015.

International Journal of Water Resources Development, 2015
Vol. 31, No. 2, 174–200, http://dx.doi.org/10.1080/07900627.2015.1020417

A comparative high-altitude meteorological analysis from three catchments in the Nepalese Himalaya

J.M. Shea[a]*, P. Wagnon[a,b], W.W. Immerzeel[c], R. Biron[b], F. Brun[b] and F. Pellicciotti[d]

[a]*International Centre for Integrated Mountain Development, Kathmandu, Nepal;* [b]*IRD/UJF–Grenoble 1/CNRS/G-INP, LTHE UMR5564, LGGE UMR5183, Grenoble, France;* [c]*Department of Physical Geography, Utrecht University, the Netherlands;* [d]*Department of Environmental Engineering, ETH Zürich, Switzerland*

(*Received 29 September 2014; accepted 14 February 2015*)

Meteorological studies in high-mountain environments form the basis of our understanding of catchment hydrology and glacier accumulation and melt processes, yet high-altitude (>4000 m above sea level, asl) observatories are rare. This research presents meteorological data recorded between December 2012 and November 2013 at seven stations in Nepal, ranging in elevation from 3860 to 5360 m asl. Seasonal and diurnal cycles in air temperature, vapour pressure, incoming short-wave and long-wave radiation, atmospheric transmissivity, wind speed, and precipitation are compared between sites. Solar radiation strongly affects diurnal temperature and vapour pressure cycles, but local topography and valley-scale circulations alter wind speed and precipitation cycles. The observed diurnal variability in vertical temperature gradients in all seasons highlights the importance of *in situ* measurements for melt modelling. The monsoon signal (progressive onset and sharp end) is visible in all data-sets, and the passage of the remnants of Typhoon Phailin in mid-October 2013 provides an interesting case study on the possible effects of such storms on glaciers in the region.

Keywords: meteorology; glaciers; water resources; monsoon; Himalaya; Nepal

Introduction

High-altitude catchments in Asia play a pivotal role in regional hydrology and water resources (Immerzeel, van Beek, & Bierkens, 2010; Viviroli, Dürr, Messerli, Meybeck, & Weingartner, 2007). Glacier melt, snow melt, and rainfall contributions to streamflow vary across the region (Lutz, Immerzeel, Shrestha, & Bierkens, 2014) and are ultimately determined by the interactions between terrain and atmospheric circulation patterns. However, future climate changes are projected to substantially impact snow and glacier water resources (Lutz et al., 2014), and warming signals appear to be enhanced at high elevations (Rangwala & Miller, 2012). Identification of glacier responses to climate change in this large and remote area is challenging, but nevertheless required to quantify glacier contribution to water resources (Immerzeel, Pellicciotti, & Bierkens, 2013; Kaser, Grosshauser, & Marzeion, 2010) and sea-level rise (Gardner et al., 2013), or to reliably project their response to twenty-first-century climate changes (Marzeion, Jarosch, & Hofer, 2012; Radić & Hock, 2011).

Glaciers are good climatic indicators (Oerlemans, 2001), and recent studies have demonstrated that glaciers across the Karakoram-Himalaya region experience contrasting patterns of volume change (Gardelle, Berthier, Arnaud, & Kääb, 2013; Kääb, Berthier,

*Corresponding author. Email: joseph.shea@icimod.org

Nuth, Gardelle, & Arnaud, 2012). Over the last decade, Karakoram glaciers have been in balanced conditions or slightly gaining mass (the so-called Karakoram anomaly; Hewitt, 2005) though glaciers in the Himalaya have been shrinking at an accelerated rate since the beginning of the twenty-first century (Azam et al., 2014a; Bolch et al., 2012). Spatial patterns of glacier change have been linked to both climatic changes (Shrestha & Aryal, 2011) and the geomorphologic characteristics of glaciers (i.e. debris-covered versus clean glaciers (Scherler, Bookhagen, & Strecker, 2011). From west to east, the region is subject to different climate systems, with an increased influence of the Asian and Indian summer monsoons and simultaneously decreased influence of westerly storm systems (Bookhagen & Burbank, 2006).

Long-term, high-resolution meteorological records at glacier elevations are an essential prerequisite to (1) place the observed glacier changes in the context of current climatic change and (2) calibrate and validate statistically and dynamically downscaled climate fields (Maussion et al., 2014; Mölg, Maussion, Yang, & Scherer, 2012), which are essential for spatially distributed models of glacier–climate response and hydrology. But in this region, where glaciers are located at high altitudes in remote environments that are difficult to access, the collection of long-term and high-quality meteorological data is challenging. Consequently, year-round meteorological observations at high-altitude glacier stations are extremely scarce in the Himalaya (Table 1), especially in comparison with other mountain regions such as the European Alps. Nevertheless, before making any projections of future glacier change, understanding how glaciers respond to the present climate is necessary, and this requires combining meteorological records at glacier elevations with glaciological monitoring.

Table 1. A summary of selected high-elevation automatic weather stations (AWS) in the HKH region, with elevation (Z) and on- or off-glacier designation, station type (A = year-round, S = seasonal/temporary), and type of observations: T = temperature, RH = relative humidity, P = precipitation, u = wind speed, θ = wind direction, $K\downarrow$ = downwelling short-wave radiation, $L\downarrow$ = downwelling long-wave radiation, p = atmospheric pressure.

Site	Z (m)	Station type	Observations	Period	Country/ source
Pyramid	5035 (off)	A	T, RH, P, u, θ, $K\downarrow$, $L\downarrow$, p	1994–2014	Nepal/1, 2
Khumbu	5350 (on)	S	T, RH, u	1999	Nepal/3
Everest S. Col	7986 (off)	S	T	1998	Nepal/4
EB050 Khumbu	5160 (on)	S	P	1976	Nepal/5
Mera	5360 (on)	A	T, RH, u, θ, $K\downarrow$, $L\downarrow$, p	2009–2010, 2012–2014	Nepal/6
AX010	4958 (off)	S	T, P	1973–1978	Nepal/7
Hidden Valley	5055 (off)	S	T, RH, P, p	1974	Nepal/8
Tibetan Plateau	4070, 4420	A	$K\downarrow$, $L\downarrow$	1998, 2003	China/9
Zhadang	5400, 5660, 5800	A	T, RH, P, u, θ, $K\downarrow$, $L\downarrow$, p	2005–2011	China/10, 11
Baltoro	5033 (on)	S	T, RH, u, θ, $K\downarrow$, $L\downarrow$, p	2004	Pakistan/12
Baltoro	4022 (off)	A	T, RH, u, θ, $K\downarrow$, $L\downarrow$, p	2004	Pakistan/12

Sources: Ageta, Ohata, Tanaka, Ikegami, and Higuchi (1980); Bollasina, Bertolani, and Tartari (2002); Diodato et al. (2012); Higuchi (1977); Higuchi, Ageta, Yasunari, and Inoue (1982); Mihalcea et al. (2006); Mölg et al. (2012); Moore and Semple (2004); Takeuchi (2000); Wagnon et al. (2013); Yang, He, Tang, Qin, and Cheng (2010); Zhang et al. (2013).

Combined glaciological and meteorological studies have already been conducted in various mountain ranges such as the Alps (Oerlemans, 2000), the Andes (Favier, Wagnon, & Ribstein, 2004; Hardy, Vuille, Braun, Keimig, & Bradley, 1998), Africa (Nicholson, Prinz, Mölg, & Kaser, 2013), and Tibet (Mölg et al., 2012; Zhang et al., 2013). Similar studies are still needed in the Karakoram-Himalaya region, though some short-term studies have been published (Azam et al., 2014b; Fujita, Sakai, & Chhetri, 1997; Immerzeel, Petersen, Ragettli, & Pellicciotti, 2014; Takahashi et al., 1987). This article presents first analyses of high-quality meteorological data-sets recorded in three distinct catchments in the Nepal Himalaya where glaciological monitoring is simultaneously performed. Long-term mass balance and meteorological observations at selected benchmark glaciers representative of various climates in Nepal are required to better understand the climate–glacier relationship and inform models and projections.

During the melt season, observations of radiative fluxes and surface height changes are required for calibration of empirical and physically based snow and ice melt models (Hock, 2005; Pellicciotti et al., 2008; Ragettli & Pellicciotti, 2012). On-glacier observations of temperature, relative humidity and wind speeds can also be used to evaluate the effect of katabatic flows on meteorological variables within the surface boundary layer (Petersen & Pellicciotti, 2011; Shea & Moore, 2010). High-altitude precipitation is perhaps the most important meteorological variable to consider with respect to both glacier mass balance and the hydrological water balance (Rasmussen et al., 2012). Gradients of precipitation in mountainous environments are subject to both vertical and horizontal variability (Barry, 2012), are affected by the mechanism of precipitation, and are often defined by an elevation of maximum precipitation. In monsoon-dominated Langtang Valley, orographic uplift and valley-scale convection result in precipitation maxima at relatively low elevations (ca. 2000 m), while winter synoptic events result in precipitation maxima at higher elevations (Bookhagen & Burbank, 2006; Immerzeel et al., 2014). However, given the uncertainties and complexity of solid precipitation analyses (Marks, Winstral, Reba, Pomeroy, & Kumar, 2013) and the limited number of stations, solid precipitation and precipitation gradients are not addressed in this study.

The main objective of this paper is to characterize and compare meteorological conditions in different high-altitude glacierized catchments in Nepal, assessed from *in situ* measurements. The following sections describe the study areas and measurements and identify data gaps and sources of error, describe the calculation of derived quantities and gradients, and compare and contrast meteorological quantities between stations and between basins. We also assess temperature and vapour pressure gradients in the Langtang catchment, and examine the high-altitude meteorological impacts of Typhoon Phailin, a large post-tropical cyclone that crossed the study area in October 2013. Based on these analyses, key points are emphasized that need to be addressed for distributed energy balance studies, glacio-hydrological modelling (spatial variability of meteorological variables), or downscaling studies.

Study area and methods

Nepal contains a glacierized area of approximately 3900 km^2 (Bajracharya, Maharjan, Shrestha, Bajracharya, & Baidya 2014; http://rds.icimod.org), 90% of which is located at elevations between 4500 and 6500 m asl. The climate in central and eastern Nepal is dominated by the Indian monsoon, with nearly 80% of total annual precipitation occurring between June and October (Bookhagen & Burbank, 2006; Wagnon et al., 2013). The Himalaya form a large orographic barrier which can produce strong horizontal and vertical

gradients of temperature and precipitation, but field-based studies of other meteorological parameters are limited. Furthermore, the climate stations operated by the Department of Hydrology and Meteorology of the Government of Nepal are mostly below 3000 m (http://www.dhm.gov.np) and thus are difficult to reconcile with high-altitude glaciological and hydrological studies.

Station locations and specifications

Combined glacier and meteorological modelling studies have been initiated by the International Centre for Integrated Mountain Development (ICIMOD) and the GLACIOCLIM project (through the Institut de Recherche pour le Développement). Through these projects, detailed meteorological observations (Table 2) have been collected at five stations, located in three catchments in Nepal: Langtang, Dudh Kosi, and Hidden Valley (Figure 1). This study compares and contrasts diurnal and seasonal patterns of air temperature (T), vapour pressure (e_a), wind speed (u), incoming solar radiation ($K\downarrow$), incoming longwave radiation ($L\downarrow$), and precipitation (P).

Meteorological observations were collected at the Kyanging and Yala Base Camp stations in Langtang Valley, at the Changri Nup and Mera Glacier stations in Dudh Kosi Valley, and at the Rikha Samba station in Hidden Valley (Figure 1). Precipitation observations were collected at Kyanging, Yala Base Camp, Yala2 and Morimoto stations in Langtang Valley, and at the Pyramid observatory near Changri Nup glacier. Station instrumentation and specifications, as well as some morphological features, are given in Table 2. All stations were off-glacier, except the Changri Nup station, which was on the debris-covered part of the glacier, and the Mera Glacier station, which was on a clean-ice glacier. The approximate measurement height at all stations was 2.0 m. The Pyramid, Yala2 and Morimoto precipitation gauges were shielded with Nipher and Tretyakov-type wind shields, respectively, while the Kyanging and Yala Base Camp precipitation sites were unshielded. A ventilated radiation shield working only during daytime was used for air temperature measurements at the Changri Nup and Mera glaciers. Meteorological observations were sampled at a frequency between 10 and 60 seconds, and recorded as 10-to-30-minute averages by Campbell Scientific and Real Time Solutions data-loggers. For all analyses in this paper, hourly averages were constructed from the data of the preceding hour.

Identification of errors

Errors in meteorological observations are not uncommon, particularly in harsh, high-elevation environments. From the five meteorological stations and three additional precipitation stations, a period of overlap from 1 December 2012 to 30 November 2013 was identified. The following steps were taken to address erroneous observations.

- Where available, data warnings and flags are used to remove spurious precipitation observations at the Pluvio sites (see Table 2).
- Night-time power losses occurred at the Changri Nup station starting in April 2013. Mean daily values at this site are used for illustrative purposes only, and when evaluating the mean daily cycle, mean hourly values are computed only for periods where more than 80% of observations are available.
- Incoming short-wave and long-wave radiation at the Mera Glacier station were affected by water ingress into the CNR4 housing. Radiation measurements from 5 September to 30 November 2013 were discarded for this analysis.

Table 2. Station locations, measurements, sensors, and morphological setting (T = temperature, RH = relative humidity, u = wind speed, θ = wind direction, $K\downarrow$ = downwelling short-wave radiation, $L\downarrow$ = downwelling long-wave radiation, P = precipitation).

Station (distance from Kyanging)	Elevation (m)	Latitude (°)	Longitude (°)	Parameters	Sensors	Morphological setting
Changri Nup (122 km)	5363	27.983	86.783	*T/RH* *u, θ* *K↓, L↓*	RMYoung 05103-5 Vaisala HMP45C Kipp&Zonen CNR4	AWS on a flat part of the debris-covered area of the glacier; valley open to the east
Mera (130 km)	5360	27.718	86.897	*T/RH* *u, θ* *K↓, L↓*	RMYoung 05103-5 Vaisala HMP155C Kipp&Zonen CNR4	AWS on Naulek Glacier (clean), drilled into the ice surface; tiltmeter
Pyramid (125 km)	5035	27.95	86.82	*P*	Geonor T-200B (shielded)	Flat grassy moraine
Kyanging	3862	28.211	85.570	*T/RH* *u, θ* *K↓, L↓* *P*	Rotronic SC2 RMYoung 015043 Kipp&Zonen CNR4 OttPluvio 400 (unshielded)	Flat grassy side-valley
Morimoto (13 km)	4919	28.253	85.682	*P*	OttPluvio 400 (shielded)	Glacier moraine crest; rocky debris
Yala Base Camp (5 km)	5090	28.233	85.612	*T/RH* *u, θ* *K↓, L↓* *P*	Rotronic SC2 RMYoung 015043 Kipp&Zonen CNR4 OttPluvio 400 (unshielded)	Bedrock knob below Yala Glacier
Yala2 (4 km)	4831	28.229	85.597	*P*	OttPluvio 400 (shielded)	Scree
Rikha Samba (212 km)	5310	28.799	83.515	*T/RH* *u* *K↓*	Rotronic SC2 RMYoung 015043 Kipp&Zonen CMP6	Scree/bedrock

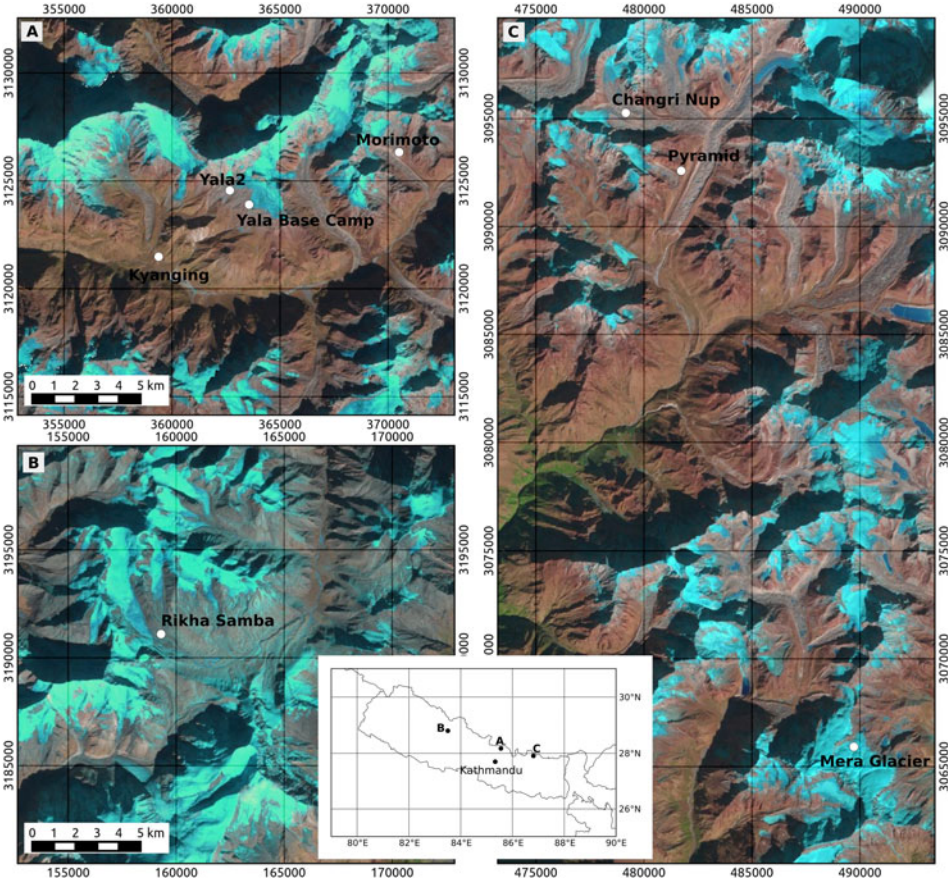

Figure 1. Location of meteorological and precipitation stations in (a) Langtang Valley, (b) Hidden Valley, and (c) DudhKosi, with location map of Nepal. Station location maps are given in UTM 45N projection.

- Values of $K\downarrow$ lower than 7 W m^{-2} are set to zero, and the maximum albedo ($\alpha = K\downarrow/K\uparrow$) was assumed to be 0.95. For observations where α exceeds 0.95 (i.e. where snowfall or dew/frost has reduced the amount of incoming solar radiation), $K\downarrow$ was recalculated as $K\uparrow/0.95$.
- Precipitation data at the Pyramid site are extracted from the bucket weight, which is recorded with a GeonorT-200B at 15-minute intervals. To extract the precipitation at each time step, we first calculate the change in bucket content, which is supposed to be always positive given that evaporation is blocked with a layer of oil spread out over the water. However, the vibrating device used to weigh the bucket is sensitive to external perturbations such as wind, which results in a background noise, i.e. small positive or negative changes for every 15-minute time step. To smooth the signal and avoid any negative precipitation values, each negative change recorded over a 15-minute time step is compensated by summing it with the neighbouring positive changes. In this way, the accumulated precipitation recorded over the entire period remains unchanged.
- While there are a number of empirical corrections for gauge undercatch based on air temperature and wind speed (Førland et al., 1996; Michelson, 2004; Wagnon et al.,

2009), these corrections need to be calibrated for different regions. Future research will be specifically focused on solid precipitation, rain/snow thresholds, and gauge undercatch issues, which do not substantially affect the results presented here.

Derived meteorological quantities and methods of comparison

To calculate vapour pressure we first calculate the saturation vapour pressure (e_s) following Teten's formulae (Bolton, 1980):

$$e_s = \begin{cases} 6.108 \times 10^{\frac{9.5T}{T+265.5}}, & T < 0 \\ 6.108 \times 10^{\frac{7.5T}{T+237.3}}, & T > 0 \end{cases} \quad (1)$$

where T is the observed air temperature in °C. Actual vapour pressure (in hPa) is calculated from e_s and relative humidity (RH), which ranges from 0 to 100%:

$$e_a = e_s RH \quad (2)$$

Bulk daily atmospheric transmissivity (τ, unitless) is calculated as the ratio between observed mean daily incoming solar radiation and mean daily extraterrestrial solar radiation ($K\downarrow_{ex}$),

$$\tau = \frac{K\downarrow}{K\downarrow_{ex}\ \tau_{cs}} \quad (3)$$

where $K\downarrow_{ex}$ (W m^{-2}) was calculated for the latitude and longitude of each site (Table 2) using the United States National Renewable Energy Laboratory's online solar calculator (http://www.nrel.gov/midc/srrl_bms/), and τ_{cs} is the clear sky atmospheric transmissivity. We estimate τ_{cs} for each site by fitting daily $K\downarrow$ observations with $K\downarrow_{ex}\tau_{cs}$. To facilitate τ comparisons with the Changri Nup record, which is missing early-morning insolation data (usually between 1 and 2 hours after sunrise) between April and October 2013, mean daily $K\downarrow_{ex}$ at Changri Nup was recalculated by excluding the morning hours when observations were missing.

To compare the seasonal and diurnal patterns of each meteorological data-set, we first divide the year into four seasons: winter (December–February), pre-monsoon (March–May), monsoon (June–September), and post-monsoon (October–November). These divisions are arbitrary, but similar to those noted by Bonasoni et al. (2010). Mean daily values and total daily P are calculated for each station to examine seasonal trends and variability. For each station we also calculate the hourly mean and standard deviation to examine diurnal cycles of temperature, vapour pressure and wind speed in each season. Wind speeds and directions at each site are also compared with wind rose plots. For each hour, season and station we define a mean precipitation intensity (mm h^{-1}) for all hourly observations where $P > 0.1$ mm ($N_{P>0.1}$), and calculate an hourly precipitation frequency as $N_{P>0.1}/N$, where N is the total number of hourly observations. Gradients of near-surface temperature (γ_T) and vapour pressure (γ_{ea}) provide important information for distributed melt models. In Langtang Valley, where two stations are separated by only 2 km horizontally but by 1300 m in elevation, γ_T and γ_{ea} are computed as:

$$\gamma_T = \frac{T_1 - T_2}{Z_1 - Z_2} \quad (4)$$

$$\gamma_{\mathrm{ea}} = \frac{ea_1 - ea_2}{Z_1 - Z_2} \tag{5}$$

where Z_1 and Z_2 are elevations of the automatic weather stations. Gradients of near-surface temperature are a large source of uncertainty in temperature-indexed hydrological models (Immerzeel et al., 2014; Petersen & Pellicciotti, 2011), and melt modelling at hourly timescales requires understanding of sub-diurnal variability in temperature lapse rates. We thus examine seasonal variations in mean daily temperature gradients, and compare hourly temperature gradients calculated (a) for each season and (b) for snow-cover conditions at the Yala Base Camp site, as the presence of snow can affect near-surface temperatures.

In energy-balance models, the calculation of both sensible and latent heat fluxes requires estimates of near-surface T and e_a. Information about γ_T can also be used to infer the elevation of the zero-degree isotherm, which affects both precipitation phase (liquid or solid) and the sign of the sensible heat flux. The vapour pressure immediately above a melting snow or ice surface at 0°C is fixed at 6.11 hPa. The elevation of the 6.11 hPa isoline (obtained from γ_{ea}) thus impacts the sign of the latent heat flux, which controls the energy gain (condensation) or loss (evaporation or sublimation) at the surface (Shea & Moore, 2010).

From the computed temperature and vapour pressure gradients, we derive the approximate elevations of the 0 °C isotherm ($Z_{T=0}$) and the 6.11 hPa isoline ($Z_{ea=6.11}$) as:

$$Z_{\mathrm{T=0}} = \frac{-T_{\mathrm{K}}}{\gamma_{\mathrm{T}}} + Z_{\mathrm{K}} \tag{6}$$

$$Z_{\mathrm{ea=6.11}} = \frac{6.11 - ea_{\mathrm{K}}}{\gamma_{\mathrm{ea}}} + Z_{\mathrm{K}} \tag{7}$$

where Z_{K} is the elevation of the Kyanging station. For glaciers in monsoon climates, these quantities provide important information about the phase of precipitation at different elevations, and have a significant control on the sign of the sensible and latent heat fluxes.

Results

Comparison of seasonal variations in meteorological components

Time series of meteorological variables recorded at the Kyanging, Yala Base Camp, Rikha Samba, and Changri Nup and Mera Glacier stations illustrate the seasonal variation of meteorological variables across the region (Figure 2).

Temperature and vapour pressure

Air temperatures at all sites are strongly correlated at daily time step ($r = 0.93–0.97$), with high variability in the post-monsoon and winter months, and reduced variability in the monsoon. Temperatures at the Changri Nup station are elevated in the pre-monsoon period (after 21 April 2013) due to the missing early-morning (approximately 03:00–07:00) data. At the Mera Glacier site, mean daily temperatures do not exceed 3°C, a consequence of excess energy at the surface being directed to snow and ice melt. Vapour pressures calculated from air temperature and relative humidity are also highly correlated at daily time step ($r = 0.95–0.97$). However, the seasonal evolution of vapour pressure is different between low elevation (Kyanging) and high elevation (Yala, Changri Nup, Rikha Samba,

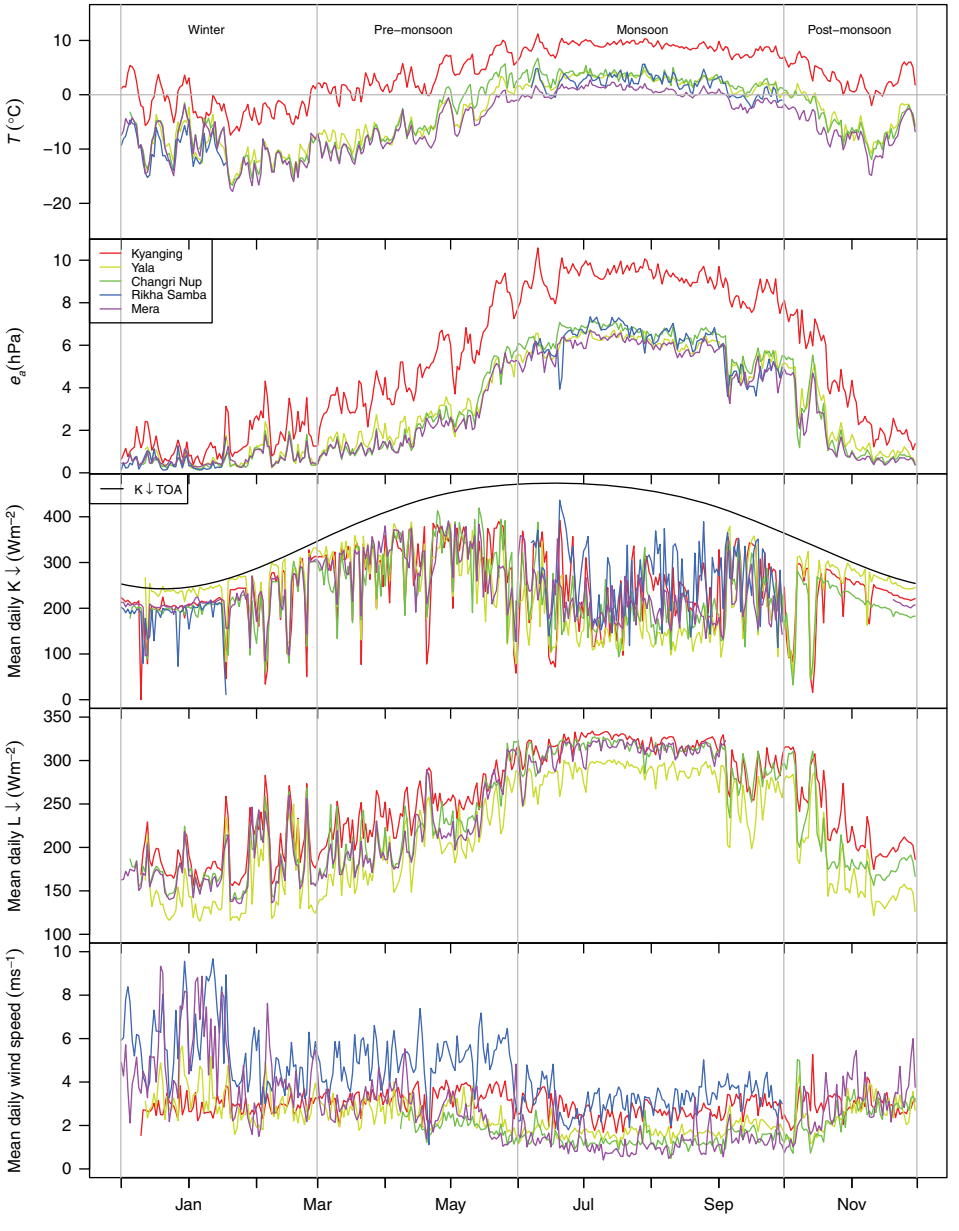

Figure 2. Summary of mean daily 2012–2013 meteorological data. From top to bottom, air temperature (T), vapour pressure (e), incoming short-wave radiation ($K\downarrow$), incoming long-wave radiation ($L\downarrow$), and wind speed (u). Climatological seasons (see text) are shown as vertical grey lines, and extraterrestrial global radiation calculated for 28N, 85E is given in black.

Mera). In winter, vapour pressures at all sites are extremely low (<2 hPa). Moisture advection and increased temperatures in the pre-monsoon season lead to elevated vapour pressures at all sites, but the increase is greatest at Kyanging. During the monsoon, vapour pressures at Kyanging remain 3–4 hPa higher than the high-elevation sites, but this difference is reduced to less than 1 hPa by the end of the post-monsoon.

Incoming short-wave and long-wave radiation

At all stations, increased cloudiness in the pre-monsoon leads to reductions in mean daily $K\downarrow$, and low values of $K\downarrow$ during the monsoon (Figure 2). Compared to incoming solar radiation at the top of the atmosphere (K_{TOA}), the Kyanging and Yala sites exhibit significantly different incoming short-wave radiation during the monsoon, which is probably related to cloud formation and valley circulation patterns. Similarly, Rikha Samba appears to have a higher mean incoming solar radiation. A sharp drop in vapour pressures at the high-elevation sites near the beginning of September corresponds with an increase in $K\downarrow$. The relative absence of clouds during the post-monsoon and winter seasons is also evident, as $K\downarrow$ parallels the extraterrestrial radiation. Correlations in mean daily $K\downarrow$ are moderate ($r = 0.55–0.80$) between the Kyanging, Yala Base Camp, Changri Nup, and Mera stations, and low ($r = 0.01–0.41$) between Rikha Samba and all other stations. The low correlations point towards the differences between cloud formation processes in windward and leeward sites, and the influence of the monsoon; Rikha Samba is the most westerly site, and is also the only site of our study located on the north side of the main mountain range, i.e. on its leeward slope.

Downwelling long-wave radiation (not measured at Rikha Samba) shows a minimum in the winter months, a gradual increase through the pre-monsoon, and a stable maximum for much of the monsoon (Figure 2). The break in the monsoon recorded in both the vapour pressure and solar radiation time series results in a steep decline in $L\downarrow$, which recovers until the end of September, and then declines rapidly during the post-monsoon period. Values for $L\downarrow$ are greatest at the lowest-elevation station (Kyanging), and lowest at the Yala station. Inter-station correlations in mean daily $L\downarrow$ range between 0.92 and 0.99 at daily time steps, and the highest correlation occurs between the Mera Glacier and Changri Nup stations.

Wind speed

Observed wind speeds are greatest at the Rikha Samba and Mera Glacier sites, and are particularly strong (greater than 4 m s^{-1}) during the winter and pre-monsoon (Figure 2). Wind speeds at all sites decrease during the monsoon, and exhibit reduced variability. Correlations in mean daily u are positive between all stations, with the greatest correlation ($r = 0.76$) between the Changri Nup and Yala Base Camp stations. The lowest correlation in mean daily u ($r = 0.10$) is found between the Kyanging and Mera Glacier stations. A surprisingly low correlation ($r = 0.26$) is also observed between the Kyanging and Yala Base Camp stations, which are only separated by 5 km horizontally (Table 2).

Precipitation

Daily precipitation totals in 2012–2013 demonstrate (1) the strong seasonality of precipitation, (2) differences in the magnitude of precipitation events between the Langtang and Dudh Kosi sites, and (3) the extraordinary precipitation amounts received during the passage of remnants of Typhoon Phailin in October 2013 (Figure 3). Winter and pre-monsoon precipitation events are sporadic, but with some significant accumulation totals, whereas precipitation occurs almost daily during the monsoon. Total annual precipitation observed at the Kyanging and Pyramid stations was 924.0 and 521.5 mm, respectively, with 56.5% and 70.0% of the precipitation occurring between June and September (Table 3). The share of monsoon precipitation in the annual total typically averages 80% in the region (Shea et al., in review; Wagnon et al., 2013). However, due to

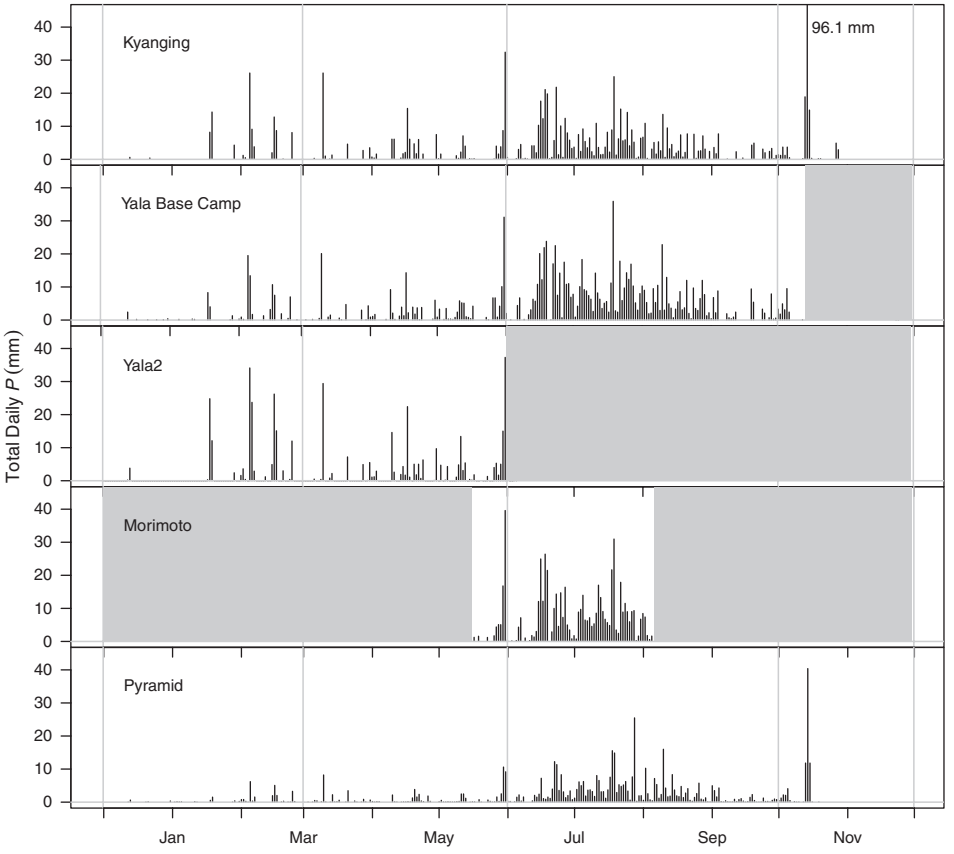

Figure 3. Total daily precipitation at Kyanging, Yala Base Camp, Yala2, Morimoto and Pyramid stations. Periods with no data are indicated in grey.

three-day precipitation totals of 129.9 mm and 63.9 mm at Kyanging and Pyramid during the Typhoon Phailin event (11–13 October 2013), the post-monsoon precipitation totals are elevated (Table 3). At Kyanging, 96.1 mm of precipitation fell during the second day of the event, and the Pluvio station at Yala overflowed during the event.

Previous studies of Kyanging meteorological data observed mean annual precipitation totals of 646.5 mm (Racoviteanu, Armstrong, & Williams, 2013), which is 30% less than that observed in this study, and a transect of tipping bucket stations in the valley recorded annual precipitation totals between 867 and 1819 mm (Immerzeel et al., 2014). While

Table 3. Seasonal and annual precipitation totals, 2012–2013. Morimoto precipitation totals were not calculated due to missing data. Relative contributions are given in parentheses for stations with a full year of data.

	Total precipitation, mm				
Site	DJF	MAM	JJAS	ON	Total
Kyanging	100.2 (11%)	136.9 (15%)	535.4 (58%)	151.5 (16%)	924.0 (100%)
Pyramid	27.0 (5%)	57.0 (11%)	371.9 (70%)	75.6 (14%)	531.5 (100%)
Yala Base Camp	85.8	157.9	746.4	–	–
Yala2	172.7	205.1	–	–	–

meteorological variability may explain some of the 30% difference between historical and 2012–2013 precipitation observations, a more likely explanation is that our measurements were automated, in contrast to the historical measurements, which were manual. Manual measurements are collected by an observer and are integrated over an approximate 24-hour period. Historical measurements may be subject to both systematic and random errors due to evaporation, measurement errors, and data transcription. This measurement bias has potentially large implications for the development, calibration and testing of hydrological and glaciological models in the region, and should be considered in future studies.

Kyanging, Yala Base Camp and Yala2 precipitation totals during the common period of record (1 December 2012–1 June 2013) are 269.5, 274.9 and 415.1 mm, respectively. The 150% higher precipitation observed during this period at the Yala2 station is probably due to the effects of the wind shield installed only at this location. Indeed, precipitation during the winter and pre-monsoon seasons occurs primarily as snowfall, and gauge accumulation totals are thus highly sensitive to wind speed (Yang, Goodison, Ishida, & Benson, 1998). Precipitation totals at Kyanging and Yala Base Camp are nearly identical during the winter and pre-monsoon but these totals are probably both under-estimated due to gauge undercatch. However, during the monsoon Yala Base Camp received 143 mm more precipitation than Kyanging – nearly 150% of the Kyanging value. This higher value, observed at two unshielded measurement sites, is probably due to orographic or convective effects that exist during the monsoon (Immerzeel et al., 2014).

Atmospheric transmissivity

Net all-wave radiation is the greatest contributor to the surface energy balance of high-altitude snowpacks and glaciers (Wagnon, Ribstein, Francou, & Pouyaud, 1999). Atmospheric transmissivity, which regulates the amount of short-wave radiation reaching the surface, is a function of atmospheric water vapour content, impurities, and clouds. As observations of short-wave radiation may be difficult to establish at high-elevation sites, atmospheric transmissivity is typically parameterized and used to scale global solar radiation at the top of the atmosphere.

Our estimates of clear-sky transmissivity (τ_{cs}) range from 0.98 (Yala Base Camp) to 0.85 (Rikha Samba). Time series of bulk daily transmissivity (τ; Figure 4) illustrates the synoptic (large-scale) nature of winter precipitation events, which result in correlated reductions in τ at the Langtang and Dudh Kosi sites. Similar reductions in transmissivity are also observed during the Typhoon Phailin event. During the pre-monsoon, steady declines in τ are observed in the Kyanging, Yala Base Camp, Mera Glacier and Changri Nup records, sporadically interrupted by sharp decreases due to precipitation events. Atmospheric transmissivity values at these sites are lowest during the monsoon, and the monsoon break in September results in sharply reduced vapour pressures (Figure 2) and a concomitant increase in atmospheric transmissivity. In contrast, transmissivity values at Rikha Samba are higher during the monsoon, and the monsoon break is not clearly defined by changes in τ.

Comparison of diurnal cycles in meteorological components

Temperature and vapour pressure

Temperature and vapour pressure exhibit strong diurnal cycles that reflect daytime solar heating (Figures 5 and 6). Minimum daily temperatures at the Yala and Kyanging sites occur at 07:00, while maximum temperatures are observed between 15:00 and 16:00.

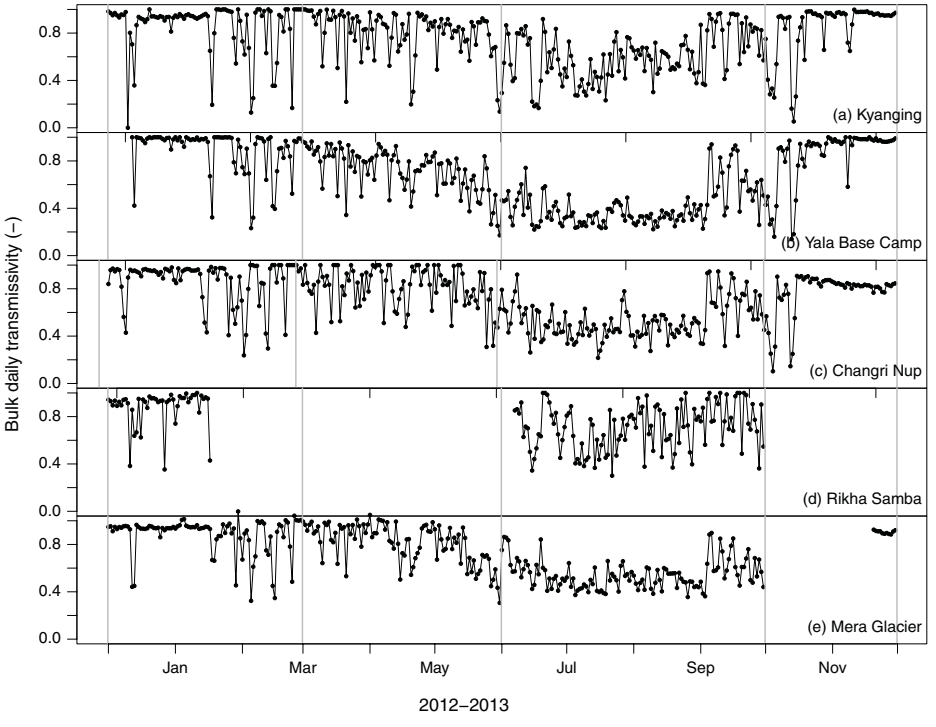

Figure 4. Bulk atmospheric transmissivity, 2012–2013, at (a) Kyanging, (b) Yala Base Camp, (c) Changri Nup, (d) Rikha Samba, and (e) Mera Glacier.

Maximum temperatures during the monsoon occur at 13:00 at Rikha Samba, and at 12:00 at Changri Nup. At all sites, the diurnal range of mean hourly air temperature (Figure 5) is strongly reduced during the monsoon. At Changri Nup, post-monsoon temperatures exhibit a marked early-afternoon maximum, in comparison with other records. Examination of the hourly records at Changri Nup suggests that this peak results from strong solar heating and relatively low wind speeds after the Typhoon Phailin snowfall event. In contrast, the daily temperature cycles at Mera Glacier show that peak temperatures occur in mid-morning (09:00), and the daily cycle is damped as surplus energy at the surface is directed to snow and ice melt, as opposed to increased air temperatures.

Vapour pressures follow a similar diurnal pattern (Figure 6), with maximum vapour pressures observed in late afternoon, and minima between 07:00 and 08:00. In pre- and post-monsoon seasons, the cycle is more gradual than that observed for temperature. Diurnal variations and absolute values of vapour pressure are lowest in winter, and the range of observed hourly vapour pressures is greatest in the post-monsoon.

Downwelling long-wave radiation

Unsurprisingly, diurnal cycles in $L\downarrow$ follow a pattern similar to mean daily temperatures and vapour pressures (Figure 7). Minimum values are observed at approximately 08:00 in all seasons, and increase towards late-afternoon/early-evening (16:00–20:00) maxima. The diurnal range and the standard deviation of observed $L\downarrow$ are lowest for the monsoon, and greatest in the post-monsoon. In the winter months, the diurnal signal of $L\downarrow$ is weak in

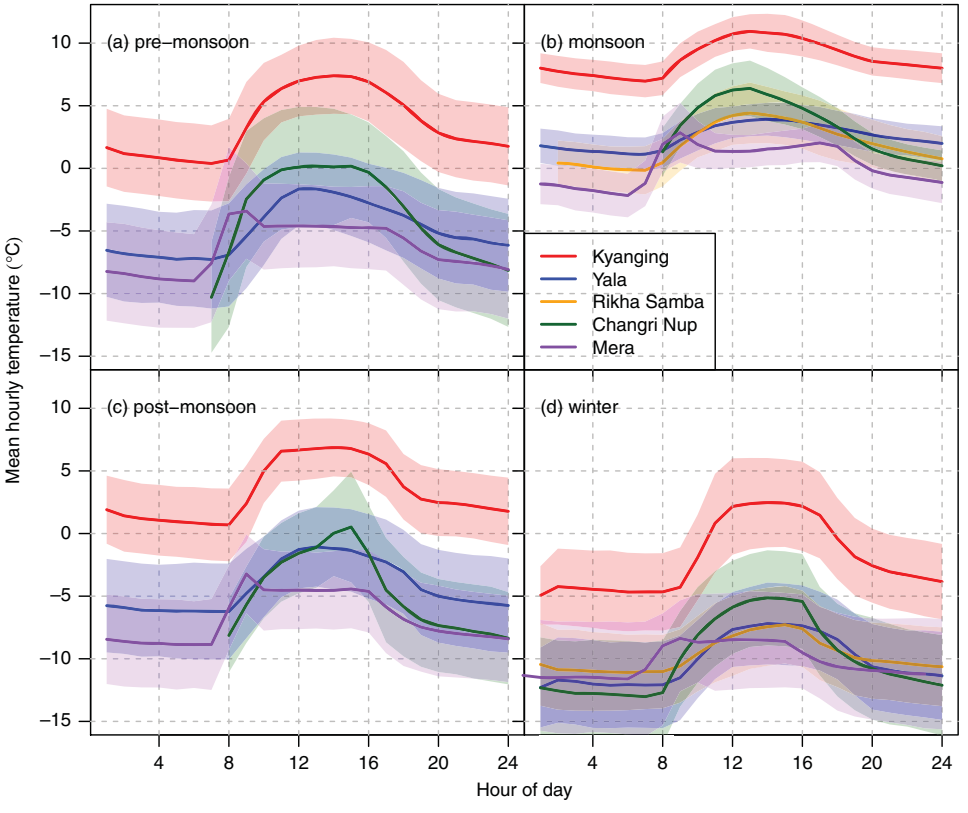

Figure 5. Cycles of mean daily temperature, for (a) pre-monsoon, (b) monsoon, (c) post-monsoon, and (d) winter. Solid lines show the hourly mean (calculated for periods where greater than 80% of observations were available), and the shaded portions give mean plus or minus standard deviation.

spite of the substantial warming observed (Figure 5) and appears to follow the vapour pressure cycle more closely. Changri Nup and Mera Glacier long-wave radiation cycles are very similar over their common periods of record.

Precipitation

At high altitudes, the timing and magnitude of precipitation can have a significant impact on glacier melt totals, as the phase is determined by air temperature. In the pre-monsoon, the frequency of precipitation is greatest in the late afternoon at all sites (Figure 8). Precipitation frequency during the monsoon is characterized by minima in the early morning (6:00–7:00), and two maxima in the mid-afternoon (13:00–16:00) and the middle of the night (23:00–2:00), with relatively high frequencies of occurrence throughout the day. In the post-monsoon and winter seasons, precipitation frequencies are generally low, with a slight tendency towards greater frequencies in the late afternoon.

Precipitation intensities are greatest in the pre- and post-monsoon seasons, with a maximum observed mean intensity of 5 mm h^{-1} at Kyanging. There do not appear to be any consistent diurnal patterns of precipitation intensity except in the pre-monsoon season, when intensities are greatest in the afternoon. Higuchi (1977) suggested that 60% of the total precipitation at Rikha Samba was received between 17:40 and 05:40. We find similar

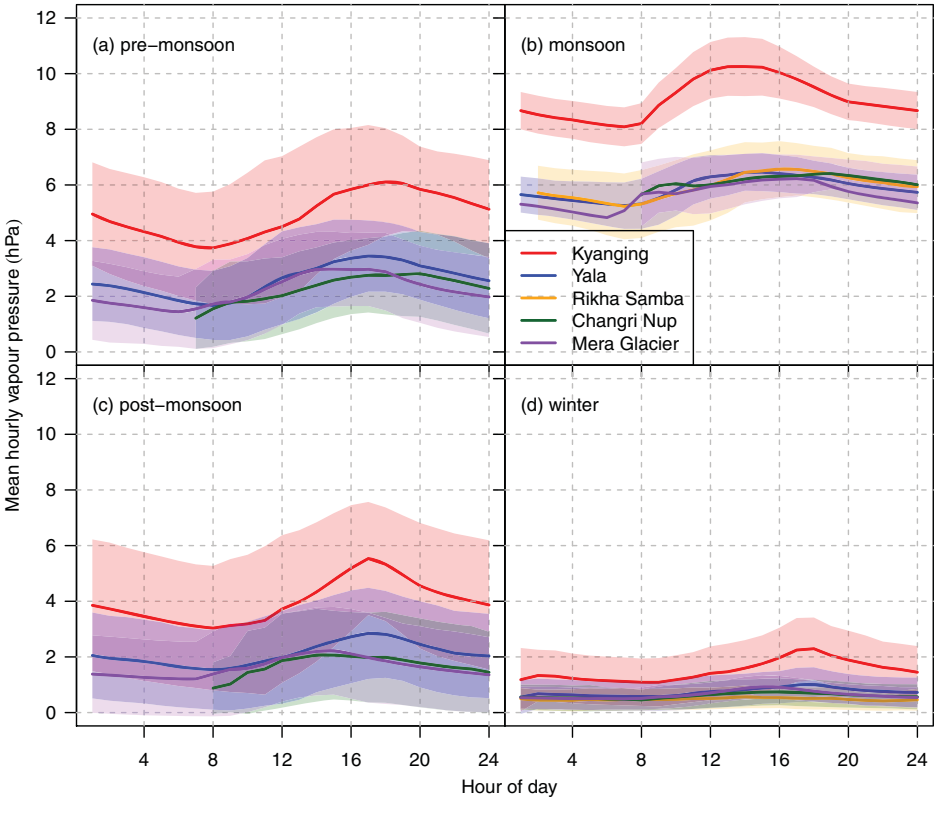

Figure 6. As in Figure 5, but for vapour pressure.

values at our stations, where between 49.3% (at Yala2) and 69.2% (at Pyramid) of total monsoon precipitation occurs between 17:00 and 05:00.

Wind speed and direction

In mountainous terrain, wind speed and direction are products of synoptic and valley-scale circulations, and topographic exposure (Whiteman, 2000). Wind speeds regulate the turbulent transfer of sensible and latent heat over melting snow and ice surfaces (Hock, 2005), but are among the most difficult meteorological parameters to model accurately in complex terrain (Jiménez et al., 2012).

Wind roses for the five sites demonstrate the dominance of valley winds at the Kyanging and Yala Base Camp stations, and the exposure of stations to synoptic-scale flows at Rikha Samba and Mera Glacier (Figure 9). Diurnal wind speed cycles are given in Figure 10. At Kyanging, the predominant wind direction is up-valley (westerly), with a secondary down-valley wind maximum. The Kyanging site (Figure 1) is above the main valley floor, on the northern slope, and daytime heating occurs in all seasons (Figure 5). Maximum mean wind speeds of 5–7 m s^{-1} occur between 15:00 and 16:00 at Kyanging. In all seasons except the post-monsoon, wind speeds at Yala Base Camp follow a similar pattern, though maximum wind speeds are lower (3–5 m s^{-1}). Wind directions at Yala Base Camp also follow a bi-modal distribution (Figure 9), with dominant up-valley (south-west) winds, and secondary down-glacier (north-east) winds.

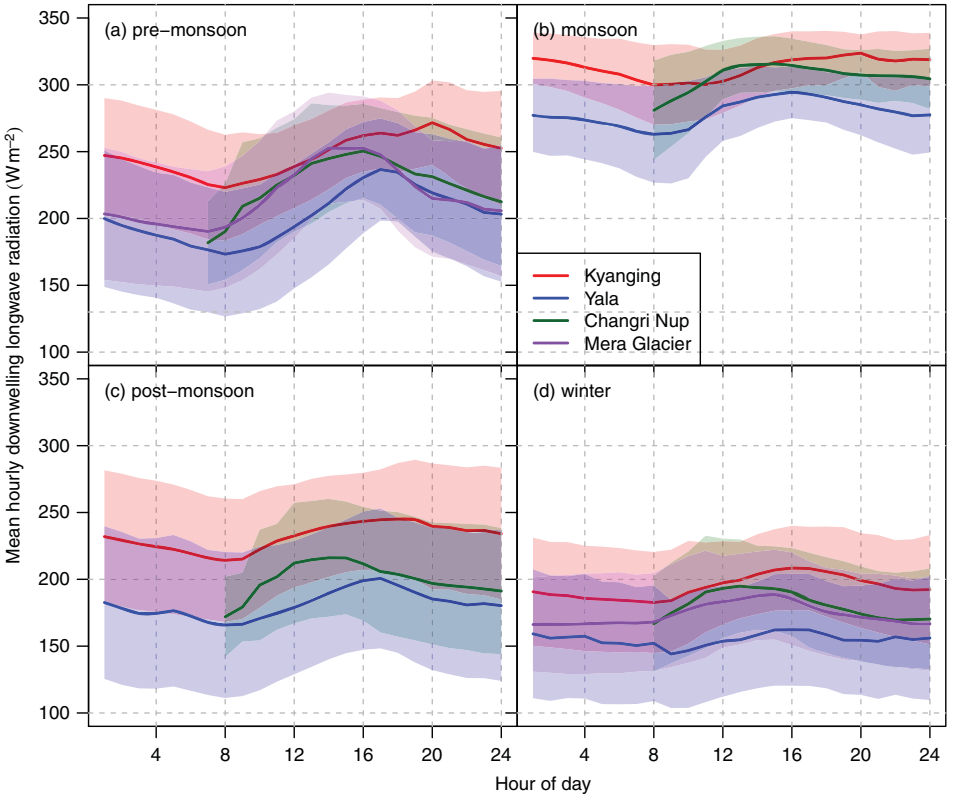

Figure 7. As in Figure 5, but for downwelling long-wave radiation. Data for the Mera Glacier station are missing in the monsoon and post-monsoon.

At Changri Nup, mid-afternoon wind maxima occur in the pre-monsoon and monsoon (Figure 10), but the maximum wind speed is the lowest of all four stations (2–3 m s^{-1}), also partly due to the fact that there is a large data gap in this series (no data between December 2012 and March 2013). Wind directions at Changri Nup are mainly from the south-west, which suggests that valley wind circulations are weak, and that this on-glacier station is influenced by glacier katabatic winds. At Rikha Samba, the distribution of wind direction is also bimodal. The dominant wind direction is from the north-west, with a secondary maximum from the south (up-valley). The greatest wind speeds, observed in winter (Figure 2), result from the channelling of synoptic-scale winds (Figure 1). At Rikha Samba, strong valley circulation results in up-valley wind maxima that average 5 m s^{-1} at 16:00 during the monsoon. Finally, at the Mera Glacier station there is no evidence of valley wind circulation. Winds are almost entirely from the west and reach up to 12 m s^{-1}, a result of the exposure of the station to synoptic-scale winds.

Temperature and vapour pressure gradients

Temperature and vapour pressure gradients computed from the hourly data observed at the Kyanging and Yala stations (Figures 11 and 12) highlight the importance of having multiple stations at different elevations. While vertical gradients would ideally be calculated with a number of stations at different elevations, this two-station gradient reflects a common measurement scenario. At daily scales, vertical temperature gradients

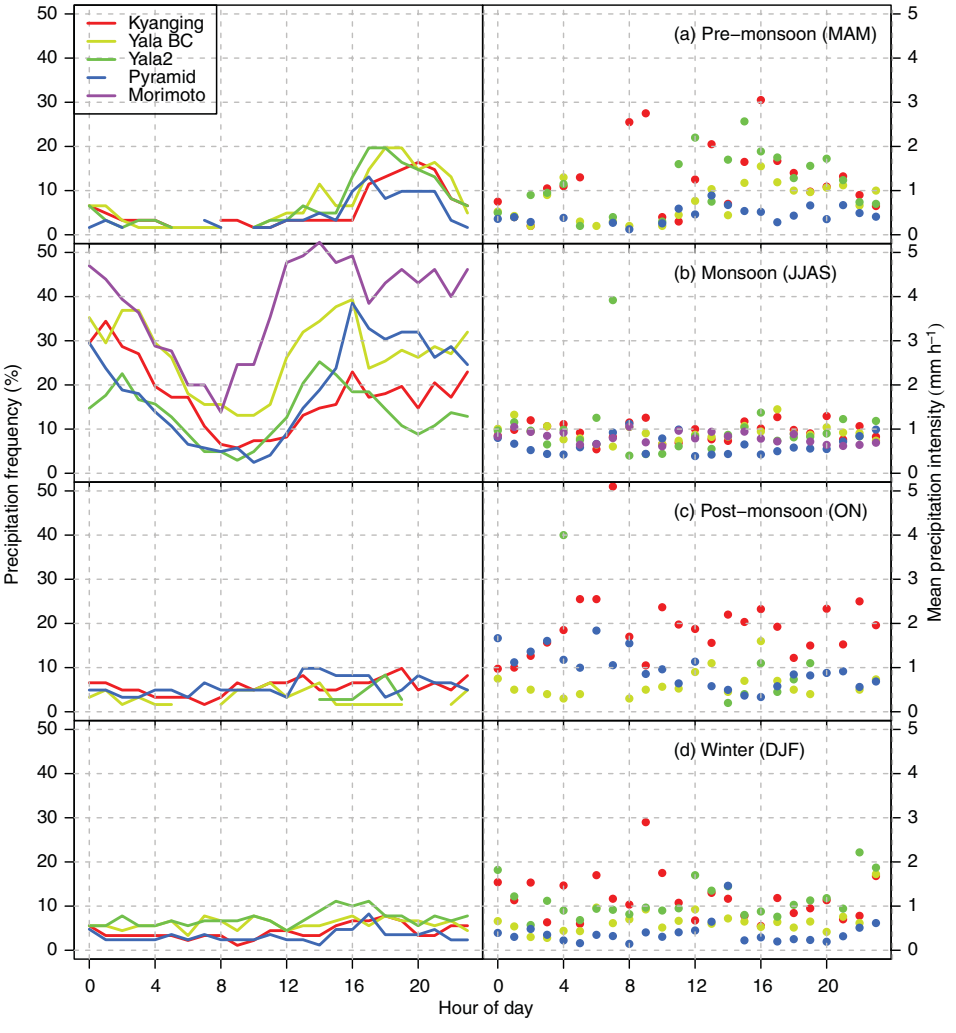

Figure 8. Hourly precipitation frequency (%, left column) and intensity (mm h^{-1}, right column) for (a) pre-monsoon, (b) monsoon, (c) post-monsoon, and (d) winter.

vary from -6 to -8°C km^{-1} during the winter and post-monsoon, and are least negative during the monsoon (-4 to -5°C km^{-1}). This is consistent with previous results reported from a transect of temperature loggers in Langtang Valley that covered a greater elevation range (Immerzeel et al., 2014), but different from the values reported by Fujita and Sakai (2000). The derived height of the estimated 0°C isotherm varies from approximately 3000 m asl in the winter to 6000 m asl during the monsoon. Glaciers in the region are situated mainly between 5000 and 6000 m (Bajracharya et al., 2014), which would suggest that a majority of glaciers in the basin experienced melt and liquid precipitation during the monsoon. During the Typhoon Phailin event in October 2013, $Z_{T=0}$ increased to 7000 m asl for a short duration.

Calculated vapour pressure gradients (Figure 12) range from 0 to -3 hPa km^{-1}, with the most negative values occurring during the monsoon. The strong gradient during monsoon results in $Z_{ea=6.11}$ values of approximately 5000 m asl, and lower values for the

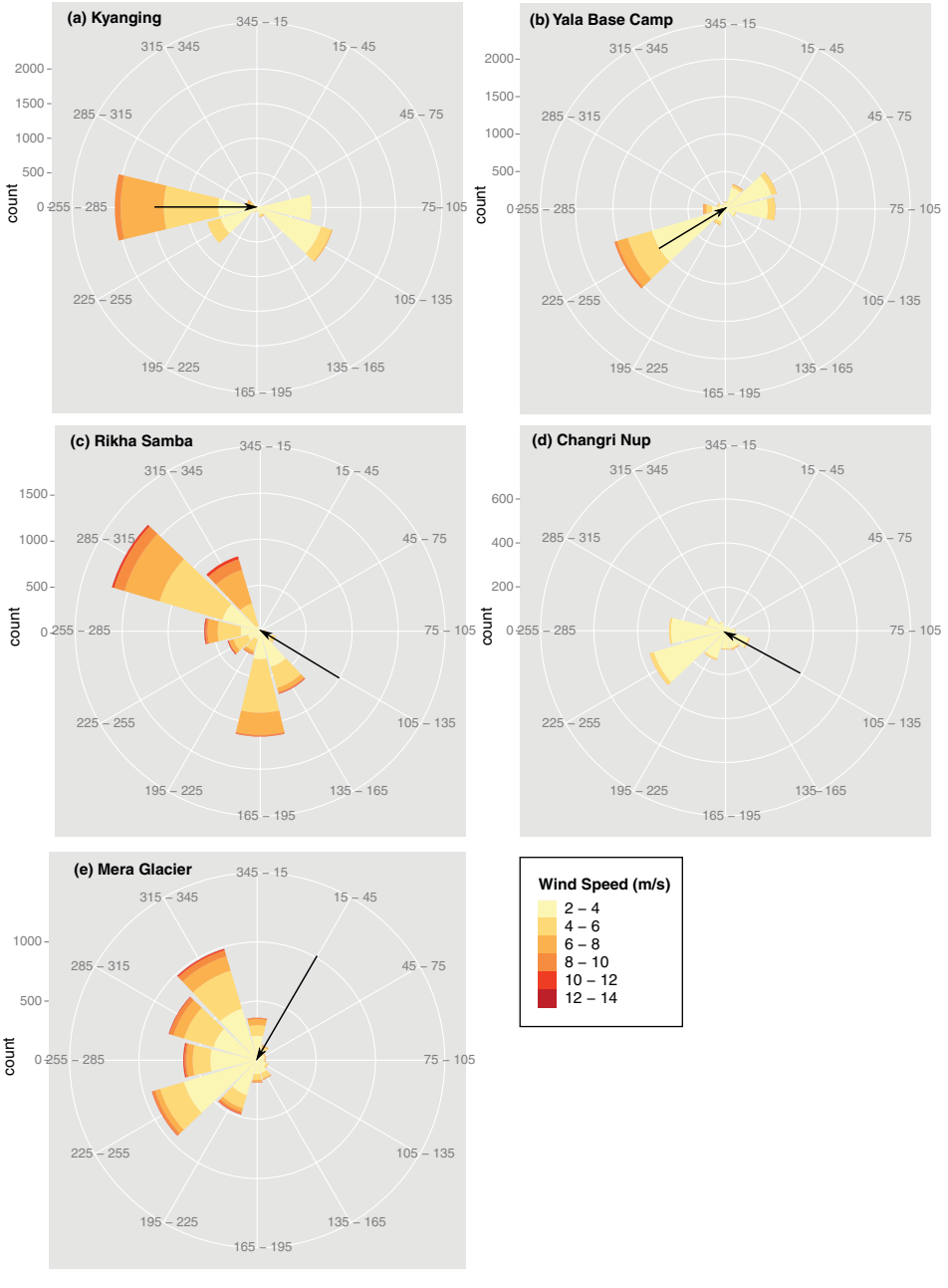

Figure 9. Wind roses for (a) Kyanging, (b) Yala Base Camp, (c), Rikha Samba, (d) Changri Nup, and (e) Mera Glacier automatic weather stations, 2012–2013. Up-valley wind directions are indicated by arrows.

rest of the year. This information suggests that glaciers in the region experience primarily evaporation/sublimation (energy loss) from the surface, which has implications for both energy balance melt models and glacier mass balance.

The diurnal cycle of hourly temperature gradients (Figure 13) calculated for the Kyanging – Yala Base is similar in all seasons and snow conditions. Vertical gradients are

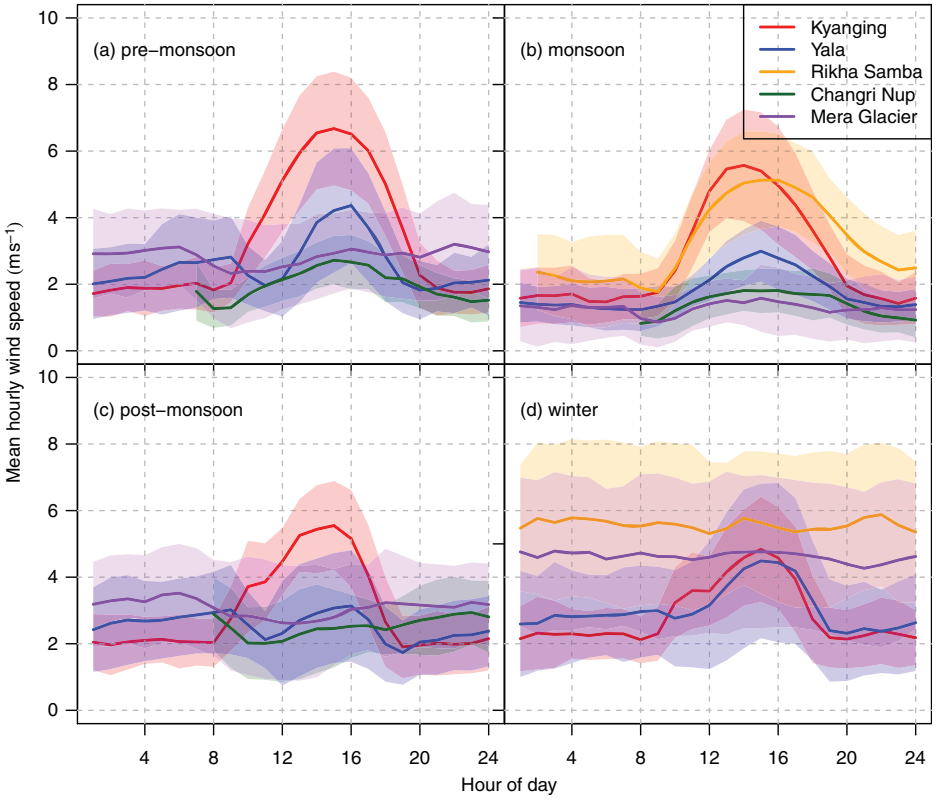

Figure 10. Mean (solid) and standard deviation (shaded) of wind speed by hour of day, for (a) pre-monsoon, (b) monsoon, (c) post-monsoon, and (d) winter seasons.

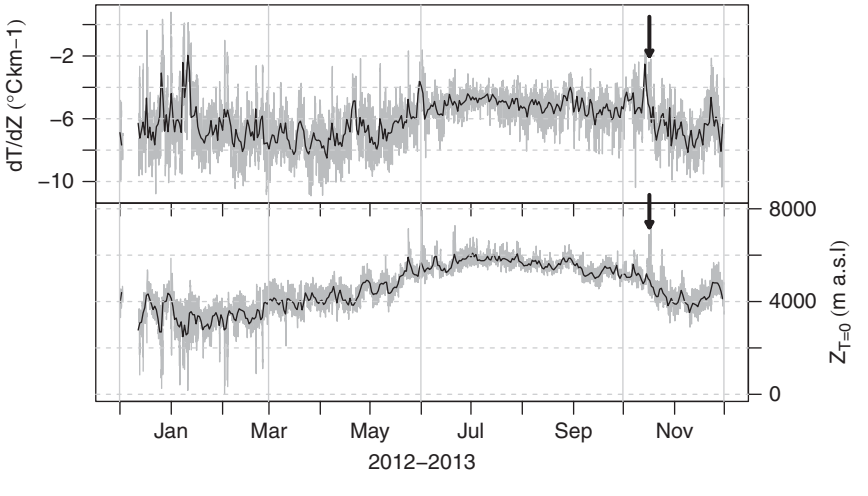

Figure 11. Temperature gradients (top panel) and height of the 0 °C isotherm (bottom panel) in the Langtang catchment, 2012–2013. Hourly values are in dark grey, and daily mean values are in black. The Typhoon Phailin event is indicated with an arrow.

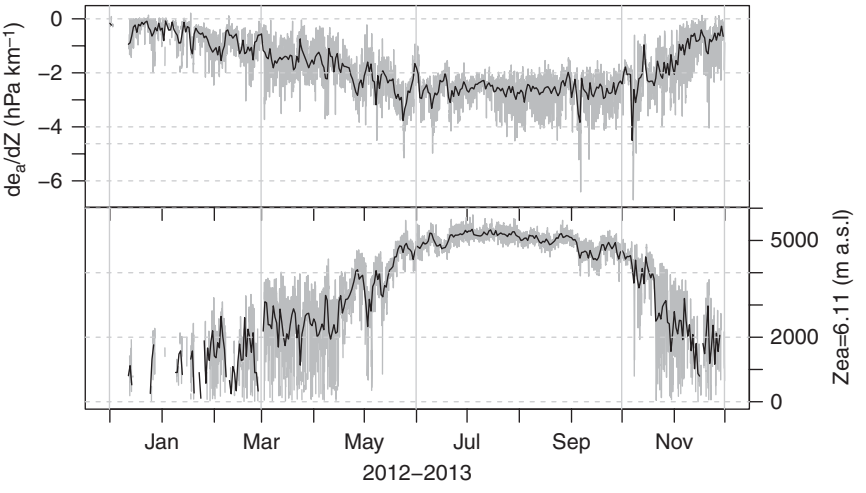

Figure 12. Gradients of vapour pressure (top panel) and height of the 6.11 hPa isoline (bottom panel) in the Langtang catchment, 2012–2013. Hourly values are in dark grey, and daily mean values are in black.

least negative at 8:00 am, and most negative in the mid-afternoon, with 1–2 °C km^{-1} differences between maximum and minimum temperature gradients. Temperature gradients are more negative when there is snow at the Yala Base Camp station, which occurs mainly during the winter and pre-monsoon months. It is probably a combination of both (a) the presence of snow that causes more negative lapse rates, and (b) the increased moisture during monsoon that results in less negative temperature gradients. Hourly temperature gradients calculated in this study show strong similarities to those reported by Fujita and Sakai (2000), though the gradients presented here are more negative.

Discussion and conclusions

Meteorological observations at high altitudes are a critical component of glacial and hydrological monitoring strategies, particularly in the Hindu Kush–Himalaya region, where standard meteorological networks exist almost exclusively at low elevations. High-altitude meteorological data are used as both input and calibration data for glacio-hydrological models (Ragettli, Pellicciotti, Bordoy, & Immerzeel, 2013) and are necessary for the evaluation of dynamically and statistically downscaled fields (Jiménez et al., 2010, Maussion et al., 2013).

Based on our analyses of seasonal and diurnal patterns of meteorological variables recorded at four stations in the Nepal Himalaya, we can make several observations that have implications for snow and ice melt modelling and dynamical downscaling. First, diurnal heating through solar radiation and valley wind circulation play significant roles in daytime temperatures and wind speed, though wind speed magnitude appears to be a function of station location in relation to the main valley axis. Both mean daily temperatures and diurnal variations are highly correlated at all sites within the study area, but sub-diurnal variations in temperature gradients (Figure 13) will strongly affect melt estimated using empirical degree-day approaches (Petersen & Pellicciotti, 2011). Wind speed extrapolations for physically based melt models or snow redistribution models remain highly uncertain.

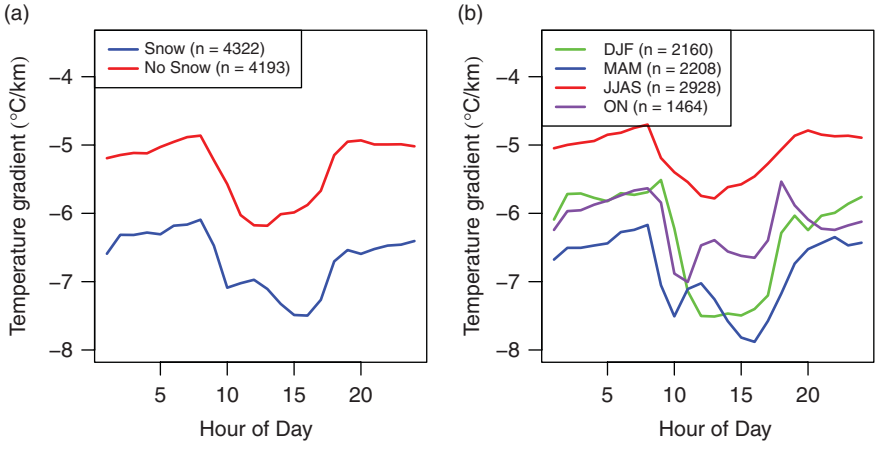

Figure 13. Mean hourly temperature gradients between Yala and Kyanging for snow-cover conditions at Yala (left), and season (right). The total number of hourly observations for each condition is given in brackets. The Yala site is snow-covered for most of the MAM period, and the latter portion of the DJF period.

Second, all sites exhibit a strong relation between daily bulk atmospheric transmissivity and vapour pressure ($r = -0.53$ to -0.83). Absorbed solar radiation at the surface is an important component of the surface energy balance at high-altitude snow and ice sites (Wagnon et al., 1999), and empirical models of atmospheric transmissivity typically rely on relatively simple measurements, such as temperature and humidity. Future research will aim to develop models of atmospheric transmissivity at these high-altitude sites and to identify the causes of different clear-sky transmissivities.

Third, our precipitation measurements support previous observations of early-morning and late-evening precipitation maxima during the monsoon in Langtang (Ueno, Shiraiwa, & Yamada, 1993). Observations from Pyramid indicate that this could be a regional phenomenon, but also raise important questions about the development of valley circulation and the precise mechanism of precipitation. At the Morimoto site, which is the farthest up-valley, the maximum precipitation frequency occurs two hours earlier than in Kyanging. Observations from multiple field trips suggest that cloud formation and condensation occur at the head of the valley first. Sustained valley circulation then drives uplift, and precipitation starts at the head of the valley before progressing to down-valley locations. Future research with high-resolution dynamical downscaling and an expanded network of precipitation stations will be able to test this hypothesis.

Fourth, the derived gradients of T, e_a and P, though computed from only two stations, shed light on the energy and mass balance of glaciers in the region. The sensible latent heat flux, for example, is expected to be positive over much of the glacierized area in the Langtang catchment as the 0 °C isotherm hovers near 6000 m asl during the monsoon. At the same time, low vapour pressure gradients during the monsoon signal that evaporation/sublimation could be an important component of the surface energy balance, as most glacierized areas will experience near-surface vapour pressures below 6.11 hPa throughout the year. Temperature gradients can also be used to identify the phase of precipitation (Higuchi, 1977) at different elevations and the resulting mass gain. Assessing the elevation of the precipitation phase change is crucial for glacier volume change studies because it has a direct impact on albedo, a key variable that controls the surface energy balance and in turn

the glacier melt. The increase in precipitation between Kyanging and Yala stations observed during the monsoon is approximately 0.19 mm m^{-1}, but this increase should not be expected to be linear over the elevation range of the catchment. Future monitoring plans in the region should strongly consider the establishment of at least two, and preferably three or more, full meteorological stations at a range of elevations so that vertical gradients can be established and hourly variability in vertical gradients assessed.

Fifth, the monsoon signal is clearly visible in nearly all of the data-sets examined here, though muted in the leeward Rikha Samba site. The monsoon exerts a strong impact on mean daily temperatures and vapour pressures, on incoming short-wave and long-wave radiation, on precipitation frequency, and even on wind speeds and directions. Local topography plays a key role in the regulation of these meteorological quantities, but the synoptic setting can be clearly established by examining multiple data-sets simultaneously. In our data-sets, we observe an asymmetric shape in the onset and finish of the monsoon (Figures 2 to 4). Indeed, during the second half of the pre-monsoon, we observe a progressive build-up of the monsoon with a regular increase in precipitation frequency, temperature, vapour pressure and downwelling long-wave radiation and a simultaneous decrease in atmospheric transmissivity, mainly due to progressively increased cloudiness blocking incoming solar radiation. Conversely, the end of the monsoon is sharp. The transition between the monsoon and post-monsoon seasons, passing from cloudy, rainy and warm to clear, dry and cold, takes no more than a few days. Consequently, changes in future monsoon onset, duration and intensity (Turner &

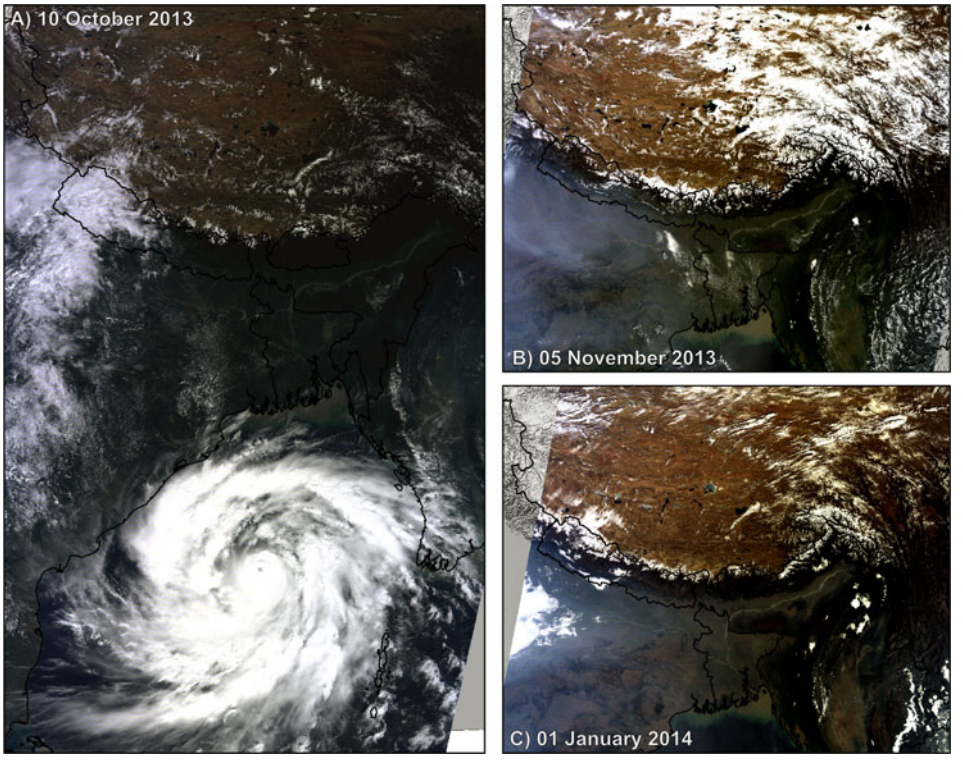

Figure 14. MODIS-TERRA RGB composites showing (a) the approach of Typhoon Phailin in the Indian Ocean, 10 October 2013; (b) extensive snow cover in middle and eastern Nepal and the Tibetan Plateau, 6 November 2013; and (c) remaining high-altitude snow cover, 1 January 2014.

Annamalai, 2012) will have significant impacts on glacier melt and accumulation processes (Diodato, Bellocchi, & Tartari, 2012).

Finally, the strong impact of the Typhoon Phailin remnants on all meteorological quantities highlights another possible area of future research. Changes in the frequency and intensity of such post-tropical storm systems may affect annual accumulation totals and glacier melt and mass balance on a regional scale. Indeed, following this rather short event (only 3 days), all the high-elevation areas of central and eastern Nepal, above approximately 4500 m asl, were covered by snow (Figure 14). In some regions this snow cover was of sufficient thickness to last until the following pre-monsoon, although the winter months are typically dry and snow cover disappears at lower elevations. Consequently, besides the direct effect on accumulation, this 3-day event affected ablation the following season. With a highly reflective snow cover on glaciers and moraine areas, melt onset was probably delayed during the following pre-monsoon period.

In conclusion, this study provides analyses of key meteorological information in a high-altitude region where data availability is severely limited. Rivers in the eastern and central Himalaya are dominated by monsoon precipitation signals (Immerzeel et al., 2013; Lutz et al., 2014), yet little is known about radiation budgets, vertical temperature and vapour pressure gradients, or precipitation mechanisms and spatial variability at high altitude. High-altitude meteorological studies are typically of limited duration, and the insights and raw data gained from our analyses can be applied to test downscaling methods and constrain key parameters in hydrological and glacier melt models. Long-term operation of these stations and their corresponding glaciological measurements will facilitate research into glacier-climate relations and long-term trends that impact regional water availability (Barry, 2012). Indeed, a regional network of high-altitude meteorological stations coupled with glacier mass balance measurements would provide critical information for future water resource assessments in the water towers of Asia.

Acknowledgements

Many thanks to an anonymous reviewer and the editor for constructive comments that have improved the original manuscript. Special thanks to Simon Wicki, Martin Heynen, Evan Miles and Eduardo Soteras for their efforts in the installation and maintenance of the Morimoto Pluvio; to Bikas Bhattarai, Sharad Joshi, Rijan Kayastha, Niraj Pradhananga and Dorothea Stumm for the installation and maintenance of the Kyanging, Yala and Rikha Samba stations; and to Yves Arnaud, Martin Ménégoz, Christian Vincent and all Pyramid staff for the installation and maintenance of Changri Nup and Pyramid Geonor stations. Yves Lejeune provided the filtered Geonor data, which is greatly appreciated. Data from the Pyramid station was made accessible through the EV-K2-CNR Project in collaboration with the Nepal Academy of Science and Technology as foreseen by a memorandum of understanding between Nepal and Italy, and thanks to contributions from the Italian National Research Council, the Italian Ministry of Education, University and Research, and the Italian Ministry of Foreign Affairs. The views and interpretations in this publication are those of the authors and are not necessarily attributable to ICIMOD.

Funding

This study was partially funded by the Netherlands Organization for Scientific Research through their VENI program and by the Research for Development (R4D) program of DFID, as well as core funds of ICIMOD (contributed by the governments of Afghanistan, Australia, Austria, Bangladesh, Bhutan, China, India, Myanmar, Nepal, Norway, Pakistan, Switzerland and the United Kingdom). The Changri Nup and Pyramid Geonor stations have been funded by the French Service d'Observation GLACIOCLIM, the French National Research Agency (ANR) through ANR-PAPRIKA, ANR-PRESHINE, and by a grant from LabexOSUG@2020 (Investissements d'avenir – ANR10 LABX56).

Supplementary information

As part of the ICIMOD publication policy, datasets used in this study will be made freely available at http://rds.icimod.org.

Disclosure statement

No potential conflict of interest was reported by the authors.

References

Ageta, Y., Ohata, T., Tanaka, Y., Ikegami, K., & Higuchi, K. (1980). Mass balance of glacier AX010 in Shorong Himal, East Nepal during the Summer Monsoon season: Glaciological expedition of Nepal, contribution no. 66. *Seppyo*, *41*, 34–41.

Azam, M. F., Wagnon, P., Vincent, C., Ramanathan, A., Linda, A., & Singh, V. B. (2014a). Reconstruction of the annual mass balance of Chhota Shigri Glacier, Western Himalaya, India, since 1969. *Annals of Glaciology*, *55*, 69–80. doi:10.3189/2014AoG66A104

Azam, M. F., Wagnon, P., Vincent, C., Ramanathan, A. L., Favier, V., Mandal, A., & Pottakkal, J. G. (2014b). Processes governing the mass balance of Chhota Shigri Glacier (Western Himalaya, India) assessed by point-scale surface energy balance measurements. *The Cryosphere Discussions*, *8*, 2195–2217. doi:10.5194/tcd-8-2867-2014

Bajracharya, S. R., Maharjan, S. B., Shrestha, F., Bajracharya, O. R., & Baidya, S. (2014). *Glacier status in Nepal and decadal change from 1980 to 2010 based on Landsat data*. Kathmandu: ICIMOD. Retrieved from: http://lib.icimod.org/record/29591/files/GSN-RR14-2.pdf

Barry, R. G. (2012). Recent advances in mountain climate research. *Theoretical and Applied Climatology*, *110*, 549–553. doi:10.1007/s00704-012-0695-x

Bolch, T., Kulkarni, A., Kääb, A., Huggel, C., Paul, F., Cogley, J. G., & … Stoffel, M. (2012). The state and fate of Himalayan glaciers. *Science*, *336*, 310–314. doi:10.1126/science.1215828

Bollasina, M., Bertolani, L., & Tartari, G. (2002). Meteorological observations at high altitude in the Khumbu Valley, Nepal, 1994–1999. *Bulletin of Glaciological Research*, *19*, 1–11.

Bolton, D. (1980). The computation of equivalent potential temperature. *Monthly Weather Review*, *108*, 1046–1053.

Bonasoni, P., Laj, P., Marinoni, A., Sprenger, M., Angelini, F. Arduini, J., … & Cristofanelli, P. (2010). Atmospheric brown clouds in the Himalayas: first two years of continuous observations at the Nepal Climate Observatory-Pyramid (5079 m). *Atmospheric Chemistry and Physics*, *10*, 7515–7531. doi:10.5194/acp-10-7515-2010

Bookhagen, B., & Burbank, D. W. (2006). Topography, relief, and TRMM-derived rainfall variations along the Himalaya. *Geophysical Research Letters*, *33*, L08405, doi:10.1029/2006GL026037

Diodato, N., Bellocchi, G., & Tartari, G. (2012). How do Himalayan areas respond to global warming? *International Journal of Climatology*, *32*, 975–982. doi:10.1002/joc.2340

Favier, V., Wagnon, P., & Ribstein, P. (2004). Glaciers of the outer and inner tropics: A different behaviour but a common response to climatic forcing. *Geophysical Research Letters*, *31*, L16403, doi:10.1029/2004GL020654

Førland, E. J., Allerup, P., Dahlström, B., Elomaa, E., Jónsson, T., Madsen, H., & … Vejen, F. (1996). Manual for operational correction of Nordic precipitation data. Report Nr. 24/96, DNMI, P.O. Box 43, Blindern, Oslo, Norway, pp. 66.

Fujita, K., Sakai, A., Air temperature environment on the debris covered area of Lirung Glacier, Langtang Valley, Nepal. Debris-Covered Glaciers (Proceedings of a workshop held at Seattle, Washington, USA, September 2000). IAHS Publ. no. 264 (pp. 83–88).

Fujita, K., Sakai, A., & Chhetri, T. B. (1997). Meterological observation in Langtang Valley, Nepal, 1996. *Bulletin of Glacier Research*, *15*, 71–78.

Gardelle, J., Berthier, E., Arnaud, Y., & Kääb, A. (2013). Region-wide glacier mass balances over the Pamir-Karakoram-Himalaya during 1999–2011. *The Cryosphere*, *7*, 1263–1286. doi:10.5194/tc-7-1263-2013

Gardner, A. S., Moholdt, G., Cogley, J. G., Wouters, B., Arendt, A. A., Wahr, J., & … Paul, F. (2013). A reconciled estimate of glacier contributions to sea level rise: 2003 to 2009. *Science*, *340*, 852–857. doi:10.1126/science.1234532

Hardy, D. R., Vuille, M. R., Braun, C. R., Keimig, F. R., & Bradley, R. S. (1998). Annual and daily meteorological cycles at high altitude on a tropical mountain. *Bulletin of the American Meteorological Society*, *79*, 1899–1913. doi:10.1175/1520-0477(1998)079<1899:AADMCA>2.0.CO;2

Hewitt, K. (2005). The Karakoram anomaly? Glacier expansion and the "elevation effect", Karakoram Himalaya. *Mountain Research and Development*, *25*, 332–340. doi:10.1659/0276-4741(2005)025[0332:TKAGEA]2.0.CO;2

Higuchi, K. (1977). Effect of nocturnal precipitation on the mass balance of the Rikha Samba Glacier, Hidden Valley, Nepal: Glaciological Expedition of Nepal, Contribution No. 38. *Seppyo*, *39*, 43–49.

Higuchi, K., Ageta, Y., Yasunari, T., & Inoue, J. (1982). Characteristics of precipitation during the monsoon season in high-mountain areas of the Nepal Himalaya. In: Hydrological Aspects of Alpine and High-Mountain Areas, IAHS Publication No. 138 (pp. 21–30).

Hock, R. (2005). Glacier melt: A review of processes and their modelling. *Progress in Physical Geography*, *29*, 362–391. doi:10.1191/0309133305pp453ra

Immerzeel, W. W., Pellicciotti, F., & Bierkens, M. F. P. (2013). Rising river flows throughout the twenty-first century in two Himalayan glacierized watersheds. *Nature Geoscience*, *6*, 742–745. doi:10.1038/ngeo1896

Immerzeel, W. W., Petersen, L., Ragettli, S., & Pellicciotti, F. (2014). The importance of observed gradients of air temperature and precipitation for modeling runoff from a glacierized watershed in the Nepalese Himalayas. *Water Resources Research*, *50*, 2212–2226. doi:10.1002/2013WR014506

Immerzeel, W. W., van Beek, L. P. H., & Bierkens, M. F. P. (2010). Climate change will affect the Asian water towers. *Science*, *328*, 1382–1385. doi:10.1126/science.1183188

Jiménez, P. A., González-Rouco, J. F., García-Bustamante, E., Navarro, J., Montávez, J. P., de Arellano, J. V. G., & Muñoz-Roldan, A. (2010). Surface wind regionalization over complex terrain: Evaluation and analysis of a high-resolution WRF simulation. *Journal of Applied Meteorology and Climatology*, *49*, 268–287. doi:10.1007/s00382-012-1326-z

Kaser, G., Grosshauser, M., & Marzeion, B. (2010). Contribution potential of glaciers to water availability in different climate regimes. *Proceedings of the National Academy of Sciences*, *107*, 20223–20227. doi:10.1073/pnas.1008162107

Kääb, A., Berthier, E., Nuth, C., Gardelle, J., & Arnaud, Y. (2012). Contrasting patterns of early twenty-first-century glacier mass change in the Himalayas. *Nature*, *488*, 495–498. doi:10.1038/nature11324

Lutz, A. F., Immerzeel, W. W., Shrestha, A. B., & Bierkens, M. F. P. (2014). Consistent increase in high Asia's runoff due to increasing glacier melt and precipitation. *Nature Climate Change*, *4*, 587–592. doi:10.1038/nclimate22372014

Marks, D., Winstral, A., Reba, M., Pomeroy, J., & Kumar, M. (2013). An evaluation of methods for determining during-storm precipitation phase and the rain/snow transition elevation at the surface in a mountain basin. *Advances in Water Resources*, *55*, 98–110. doi:10.1016/j.advwatres.2012.11.012

Marzeion, B., Jarosch, A. H., & Hofer, M. (2012). Past and future sealevel change from the surface mass balance of glaciers. *The Cryosphere*, *6*, 1295–1322. doi:10.5194/tc-6-1295-2012

Maussion, F., Scherer, D., Mölg, T., Collier, E., Curio, J., & Finkelnburg, R. (2014). Precipitation seasonality and variability over the Tibetan plateau as resolved by the High Asia Reanalysis. *Journal of Climate*, *27*, 1910–27. doi:10.1175/JCLI-D-13-00282.1.

Michelson, D. B. (2004). Systematic correction of precipitation gauge observations using analyzed meteorological variables. *Journal of Hydrology*, *290*, 161–177. doi:10.1016/j.jhydrol.2003.10.005

Mihalcea, C., Mayer, C., Diolaiuti, G., Lambrecht, A., Smiraglia, C., & Tartari, G. (2006). Ice ablation and meteorological conditions on the debris-covered area of Baltoro glacier, Karakoram, Pakistan. *Annals of Glaciology*, *43*, 292–300. doi:10.3189/172756406781812104

Moore, G. W. K., & Semple, J. L. (2004). High Himalayan meteorology: Weather at the South Col of Mount Everest. *Geophysical Research Letters*, *31*, L18109, doi:10.1029/2004GL020621

Mölg, T., Maussion, F., Yang, W., & Scherer, D. (2012). The footprint of Asian monsoon dynamics in the mass and energy balance of a Tibetan glacier. *The Cryosphere*, *6*, 1445–1461. doi:10.5194/tc-6-1445-2012

Nicholson, L. I., Prinz, R., Mölg, T., & Kaser, G. (2013). Micrometeorological conditions and surface mass and energy fluxes on Lewis Glacier, Mt Kenya, in relation to other tropical glaciers. *The Cryosphere*, *7*, 1205–1225. doi:10.5194/tc-7-1205-2013

Oerlemans, J. (2000). Analysis of a 3 year meteorological record from the ablation zone of Morteratschgletscher, Switzerland: Energy and mass balance. *Journal of Glaciology*, *46*(571–579).

Oerlemans, J. (2001). Glaciers and climate change. Lisse: A.A. Balkema.

Pellicciotti, F., Helbing, J., Rivera, A., Favier, V., Corripio, J., Araos, J., & … Carenzo, M. (2008). A study of the energy balance and melt regime on Juncal Norte Glacier, semi-arid Andes of central Chile, using melt models of different complexity. *Hydrological Processes*, *22*, 3980–3997. doi:10.1002/hyp.7085

Petersen, L., & Pellicciotti, F. (2011). Spatial and temporal variability of air temperature on a melting glacier: atmospheric controls, extrapolation methods and their effect on melt modeling, Juncal Norte Glacier, Chile. *Journal of Geophysical Research: Atmospheres (1984–2012)*, *116*, doi:10.1029/2011JD015842

Racoviteanu, A. E., Armstrong, R., & Williams, M. W. (2013). Evaluation of an ice ablation model to estimate the contribution of melting glacier ice to annual discharge in the Nepal Himalaya. *Water Resources Research*, *49*, 5117–5133. doi:10.1002/wrcr.20370

Radić, V., & Hock, R. (2011). Regionally differentiated contribution of mountain glaciers and ice caps to future sea-level rise. *Nature Geoscience*, *4*, 91–94. doi:10.1038/NGEO1052

Ragettli, S., & Pellicciotti, F. (2012). Calibration of a physically based, spatially distributed hydrological model in a glacierized basin: On the use of knowledge from glaciometeorological processes to constrain model parameters. *Water Resources Research*, *48*(3), doi:10.1029/2011WR01055

Ragettli, S., Pellicciotti, F., Bordoy, R., & Immerzeel, W. W. (2013). Sources of uncertainty in modeling the glaciohydrological response of a Karakoram watershed to climate change. *Water Resources Research*, *49*, 6048–6066. doi:10.1002/wrcr.20450

Rangwala, I., & Miller, J. R. (2012). Climate change in mountains: A review of elevation-dependent warming and its possible causes. *Climatic Change*, *114*, 527–547. doi:10.1007/s10584-012-0419-3

Rasmussen, R., Baker, B., Kochendorfer, J., Meyers, T., Landolt, S., Fischer, A. P., & … Gutmann, E. (2012). How well are we measuring snow: The NOAA/FAA/NCAR winter precipitation test bed. *Bulletin of the American Meteorological Society*, *93*, 811–829. doi:10.1175/BAMS-D-11-00052.1

Scherler, D., Bookhagen, B., & Strecker, M. R. (2011). Spatially variable response of Himalayan glaciers to climate change affected by debris cover. *Nature Geoscience*, *4*, 156–159. doi:10.1038/ngeo1068

Shea, J. M., & Moore, R. D. (2010). Prediction of spatially distributed regional-scale fields of air temperature and vapor pressure over mountain glaciers. *Journal of Geophysical Research: Atmospheres*, *115*(D23), doi:10.1029/2010JD014351

Shrestha, A. B., & Aryal, R. (2011). Climate change in Nepal and its impact on Himalayan glaciers. *Regional Environmental Change*, *11*, 65–77. doi:10.1007/s10113-010-0174-9

Takahashi, S., Motoyama, H., Kawashima, K., Morinaga, Y., Seko, K., Iida, H., & Turadahr, N. R. (1987). Meteorological features in Langtang Valley, Nepal, 1985–1986. *Bulletin of Glacier Research*, *5*, 35–40.

Takeuchi, Y. (2000). Practical prediction of ice melting beneath various thickness of debris cover on Kliumbu Glacier, Nepal, using a positive degree-day factor. In: Debris-covered Glaciers (Proceedings of an International Workshop Held at the University of Washington in Seattle, Washington, USA, 13-15 September 2000) IAHS Publ. No. 264 (pp. 53–61).

Turner, A. G., & Annamalai, H. (2012). Climate change and the South Asian summer monsoon. *Nature Climate Change*, *2*, 587–595. doi:10.1038/NCLIMATE1495

Ueno, K., Shiraiwa, T., & Yamada, T. (1993). Precipitation Environment in the LangtangValley, Nepal. In: Snow and Glacier Hydrology (Proceedings of the Kathmandu Symposium, November 1992). IAHS Publ. No. 218 (pp. 207–219).

Viviroli, D., Dürr, H. H., Messerli, B., Meybeck, M., & Weingartner, R. (2007). Mountains of the world, water towers for humanity: Typology, mapping, and global significance. *Water Resources Research*, *43*, W07447–n/a. doi:10.1029/2006WR005653

Wagnon, P., Lafaysse, M., Lejeune, Y., Maisincho, L., Rojas, M., & Chazarin, J. P. (2009). Understanding and modeling the physical processes that govern the melting of snow cover in a

tropical mountain environment in Ecuador. *Journal of Geophysical Research: Atmospheres* (1984–2012), *114*(D19), doi:10.1029/2009JD012292

Wagnon, P., Ribstein, P., Francou, B., & Pouyaud, B. (1999). Annual cycle of energy balance of Zongo glacier, Cordillera Real, Bolivia. *Journal of Geophysical Research: Atmospheres* (1984–2012), *104*, 3907–3923.

Wagnon, P., Vincent, C., Arnaud, Y., Berthier, E., Vuillermoz, E., Gruber, S., & … Pokhrel, B. K. (2013). Seasonal and annual mass balances of Mera and Pokalde glaciers (Nepal Himalaya) since 2007. *The Cryosphere*, *7*, 1769–1786. doi:10.5194/tc-7-1769-2013

Whiteman, C. D. (2000). *Mountain meteorology: fundamentals and applications*. Oxford: Oxford University Press.

Yang, D., Goodison, B. E., Ishida, S., & Benson, C. S. (1998). Adjustment of daily precipitation data at 10 climate stations in Alaska: Application of World Meteorological Organization intercomparison results. *Water Resources Research*, *34*, 241–256. doi:10.1029/97WR02681

Yang, K., He, J., Tang, W., Qin, J., & Cheng, C. C. (2010). On downward shortwave and longwave radiations over high altitude regions: Observation and modeling in the Tibetan Plateau. *Agricultural and Forest Meteorology*, *150*, 38–46. doi:10.1016/j.agrformet.2009.08.004

Zhang, G., Kang, S., Fujita, K., Huintjes, E., Xu, J., Yamazaki, T., & … Yao, T. (2013). Energy and mass balance of Zhadang Glacier surface, central Tibetan Plateau. *Journal of Glaciology*, *59*, 137–148. doi:10.3189/2013JoG12J152